Modelling of the interaction between ELMs and fast-ions using MEGA

J. Dominguez-Palacios[1], S. Futatani[2], J. Gonzalez-Martin[1,3], M. Garcia-Munoz[1], M. Toscano-Jimenez[1], E. Viezzer[1], Y. Todo[4], Y. Suzuki[4], H. Chen[1], J. Galdon-Quiroga[1], P. Oyola[1], J.F. Rivero-Rodriguez [1], the ASDEX Upgrade* and EUROfusion MST1† Teams

[1] *University of Seville, Seville, Spain*

[2] *Universitat Politècnica de Catalunya, Barcelona, Spain*

[3] *University of California, Irvine, United States*

[4] *National Institute for Fusion Science, Toki, Japan*

Introduction

Edge localized modes (ELMs) [1] are quasiperiodic magnetohydrodynamic (MHD) instabilities that routinely appear in H-mode plasmas, driven by large edge pressure gradients and current densities. They expel particles and heat towards the first wall, reducing the lifetime of plasma-facing components and could limit the performance of future fusion devices [2]. Thus, a detailed understanding of ELM control and mitigation techniques is needed.

Recent experimental observations have revealed that ELMs interact strongly with the energetic-ion population at the plasma edge. Fast-ion loss detector (FILD) measurements have shown energetic-ion losses [3] and acceleration [4] during ELMs. The impact that this interaction between fast-ions and ELMs may have on the ELM itself, and its implications towards the development of a robust ELM control technique, is still unknown. Therefore, to understand the interaction between ELMs and fast-ions, the kinetic effects of energetic-ions should be included in non-linear MHD models of ELMs. In this work, the non-linear hybrid kinetic-MHD code MEGA [5] has been applied for an ASDEX Upgrade (AUG) plasma to investigate the interplay between ELMs and fast-ions.

1 Simulation set up

The MEGA code is a hybrid-MHD code in which the MHD and fast-ion dynamics are coupled through the energetic-ion current density in the MHD momentum equation. MEGA solves the full MHD equations starting from an initial equilibrium. The δf method [6–8] is used to solve the kinetic equation of fast-ions, adopting the drift kinetic description and including Finite Larmor Radius (FLR) effects [9].

*See the author list of H. Meyer *et al.*, Nucl. Fusion **59**, 112014 (2019).

†See the author list of B. Labit *et al.*, Nucl. Fusion **59**, 086020 (2019).

The equilibrium profiles and geometry are taken from the AUG discharge #33616 at 7.2 s [10], as shown in figure 1a. The equilibrium reconstruction is performed with the CLISTE code [11], which takes into account the measured kinetic profiles. In these MEGA simulations, the resistivity is given by $\eta(T) = \eta_0 (T/T_0)^{-3/2}$, where $T_0 = 2T_{e,0} = 6.6$ keV is the temperature at the magnetic axis and $\eta_0 = 10^{-7}\Omega$m $\approx 20\eta_{\text{Spitzer}}$ is the central resistivity. The viscosity follows the same profile, which leads to a constant magnetic Prandtl number, $\text{Pr}_\text{m} = 10$. The particle and perpendicular thermal diffusivity are given by an ad-hoc profile to mimic the edge transport barrier [12]. The parallel thermal diffusivity is given by $\chi_\parallel = \chi_{\parallel_0} (T/T_0)^{5/2}$, with $\chi_{\parallel_0} = 3.6 \times 10^5$ m^{2}s^{-1}. The profiles of these parameters are shown in figure 1b.

The initial fast-ion distribution is an off-axis anisotropic slowing down distribution. The realistic off-axis part of the fast-ion distribution is considered in the energetic particle pressure profile, which is $p_{\text{EP}} = \beta_{\text{EP}} \frac{B_0^2}{2\mu_0} \exp\left[-\left(\frac{\Psi_\text{N}-\Psi_{\text{N}_0}}{\sigma_{\Psi_\text{N}}}\right)^2\right]$, with $\beta_{\text{EP}} = 0.01$ the ratio between fast-ion and magnetic pressures, Ψ_N the normalized poloidal flux, $\Psi_{\text{N}_0} = 0.55$ the center of the off-axis and $\sigma_{\Psi_\text{N}} = 0.3$ the spatial width. The anisotropic slowing down component of the distribution is given by $f(v,\Lambda) = \frac{1}{v^3+v_{\text{crit}}^3}\frac{1}{2}\text{erfc}\left(\frac{v-v_{\text{birth}}}{\Delta_v}\right)\exp\left[-\left(\frac{\Lambda-\Lambda_0}{\Delta_\Lambda}\right)^2\right]$, with $\Lambda = \frac{\mu B_0}{E}$ the pitch angle variable, $\Delta_v = 0.05 v_\text{A}$ the distribution width in velocity space, $v_\text{A} = 4.4 \times 10^6$ ms^{-1} the Alfvén velocity at the magnetic axis, $\Lambda_0 = 0.5$ the pitch angle for the distribution peak and $\Delta_\Lambda = 0.2$ the distribution width.

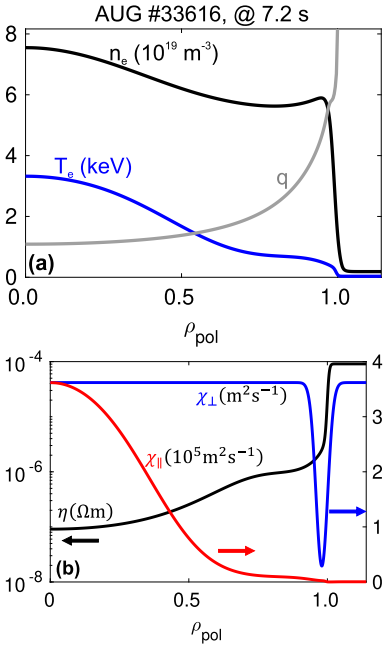

Figure 1: Initial kinetic profiles (a). Resistivity (black), perpendicular (blue) and parallel (red) thermal diffusivities (b).

The number of grid points is $N_R \times N_\phi \times N_z = 512 \times 16 \times 512$. The toroidal angle ranges from 0 to $2\pi/n$, with $n = 10$ in this paper. The number of computational particles for the kinetic model is 1.8×10^6.

2 Simulation results

Hybrid kinetic-MHD simulations of ELMs were performed to clarify the mechanism behind the interaction between ELMs and fast-ions. In figure 2, the time evolution of the energy of the $n = 10$ mode is shown for different values of the NBI injection energy. The temporal evolution of the ELM crash changes significantly with and without fast-ions and depends on the energetic-particles energy at fixed fast-ion pressure. The linear growth rate of the mode decreases as we increase E_{birth}, as seen in the inserted figure 2. The mode evolution is hardly affected by fast-ions when $E_{\text{birth}} > 90$ keV, and for lower values of E_{birth} the mode energy takes larger values.

The presence of fast-ions affects the ballooning mode structure, and their effects depend on the energy of the particles. In figures 3a and 3b, the ballooning structures with and without fast-ions in the poloidal plane are compared. In the presence of energetic particles, the ELM ballooning structures are sheared. In figures 3c and 3d, the fast-ion pressure in the poloidal plane is shown for $E_{\text{birth}} = 30$ keV and $E_{\text{birth}} = 60$ keV. The figures indicate that the ELM affects the fast-ion population at the edge, redistributing them according to the ballooning mode structure. The ELM induced fast-ion transport and loss observed in the simulations depends on E_{birth} as well.

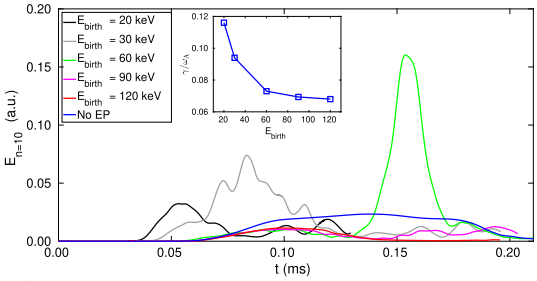

Figure 2: Time evolution of $n = 10$ mode energy and linear growth rate vs E_{birth}. The case without fast-ions (blue) is shown as well.

To understand the interaction mechanism between the ELMs and fast-ions, the dynamics of fast-ions must be analyzed in the phase-space of energetic-ions. In figures 4a and 4b, the power transfer and weight of the particles are shown for $E_{\text{birth}} = 30$ keV, selecting the particles that have the largest energy exchange $\left[\mu = (8.5-9.5)\times 10^{-16}\text{J/T}\right]$. The power transfer is $P_{\text{h}} = \sum_l w_l \frac{dE_l}{dt}$ [13], with $w_l = V_l \delta f$ the weight of the l-th particle, V_l the phase-space volume, δf the fast-ion distribution perturbation and $\frac{dE_l}{dt}$ the time derivative of the kinetic energy of the l-th particle. If $P_{\text{h}} < 0$ (> 0), then energetic-ions are giving (gaining) energy to (from) the wave. In the figures, the black lines represent the resonance condition $\omega_n - n\omega_\phi - p\omega_\theta \approx 0$. As the phase-space structures fall along resonance lines [here, $p \in (14-20)$], the interaction between ELMs and fast-ions is resonant. The particles redistribute in the phase-space along $E' = E - \frac{\omega_n}{n} P_\phi$ in figure 4b, which is a constant of motion.

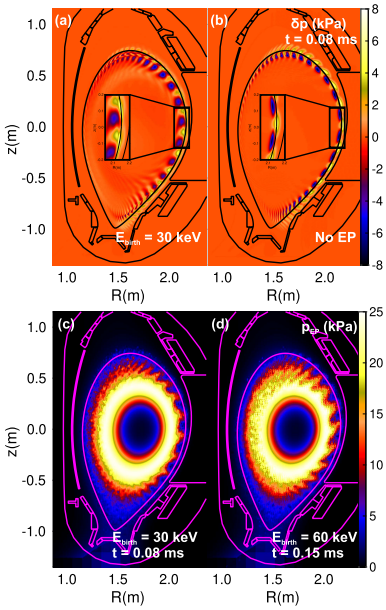

Figure 3: Top row shows pressure perturbation for $E_{\text{birth}} = 30$ keV (a) and for the natural ELM case (b). Bottom row shows the fast-ion pressure profile for $E_{\text{birth}} = 30$ keV (c) and $E_{\text{birth}} = 60$ keV (d).

A preliminary estimation of an efficient interaction between ELMs and fast-ions in ITER machine has been performed. For the standard H-mode of ITER [15], the energetic-ion orbit width normalized by the perpendicular wavelength of an $n = 10$ edge ballooning mode [14] is $q\rho_{\|}/\lambda_{\perp} \sim 0.4-0.8$ for NBI driven fast-ions and fusion born α particles, whereas for AUG, $q\rho_{\|}/\lambda_{\perp} \sim 1-2$. Here, $\rho_{\|} = \frac{m_{\text{h}} v_{\|}}{q_{\text{h}} B}$ is the parallel Larmor radius of the particles. This means the orbits would intersect the localization region of the mode; therefore, energetic particles and ELMs could interact with each other.

3 Conclusions

In this work, the ELM crash has been successfully simulated with MEGA including fast-ion effects. An impact of the energetic particles on the ELM was observed, including the linear growth rate, saturated mode energy and ballooning structure. The interaction between energetic particles and ELMs is predominantly resonant and is weakened as the energy of fast-ions increases due to the larger orbit widths. Finally, a simple analysis based on the comparison between the energetic-ion orbit width and the ballooning mode wavelength suggests that there could be a significant interaction between ELMs and fast-ions in ITER standard H-mode plasmas.

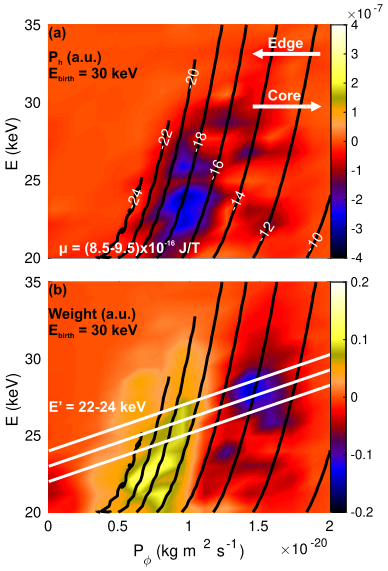

Figure 4: Power transfer (a) and weight (b) at $t = 0.08$ ms for $E_{\text{birth}} = 30$ keV. The resonances (black lines) are labeled by the bouncing harmonic p in (a) and E' (white lines) are shown in (b).

Acknowledgments

This work received funding from the Spanish Ministry of Science under grant No. FPU17/05703. This work has been carried out within the framework of the EUROfusion Consortium and has received funding from the Euratom research and training programme 2014-2018 and 2019- 2020 under Grant Agreement No. 633053. The views and opinions expressed herein do not necessarily reflect those of the European Commission. The author acknowledges the support from Marconi and MareNostrum IV, for its provision of computing resources. The author acknowledges Dr. M. Hoelzl and Dr. M. Dunne for providing input files and for fruitful discussions.

References

[1] H. Zohm, Plasma Phys. Control. Fusion **38**, 105 (1996).

[2] R.P. Wenninger *et al.*, Nucl. Fusion **54**, 114003 (2014).

[3] M. Garcia-Munoz *et al.*, Nucl. Fusion **53**, 123008 (2013).

[4] J. Galdon-Quiroga *et al.*, Phys. Rev. Lett. **121**, 025002 (2018).

[5] Y. Todo *et al.*, Phys. Plasmas **5**, 1321 (1998).

[6] S.E. Parker and W.W. Lee, Phys. Fluids B **5**, 77-86 (1993).

[7] A.M. Dimits and W.W. Lee, J. Comput. Phys. **107**, 309-323 (1993).

[8] A.Y. Aydemir, Phys. Plasmas **1**, 822 (1994).

[9] W.W. Lee, J. Comput. Phys. **72**, 243 (1987).

[10] A.F. Mink *et al.*, Nucl. Fusion **58**, 026011 (2018).

[11] P.J. McCarthy, Phys. Plasmas **6**, 3554 (1999).

[12] E. Viezzer, Nucl. Fusion **58**, 026031 (2018).

[13] A. Bierwage *et al.*, Phys. Plasmas **23**, 042512 (2016).

[14] J.A. Morales *et al.*, Phys. Plasmas **23**, 042513 (2016).

[15] A.C.C. Sips *et al.*, Plasma Phys. Control. Fusion **47**, A19 (2005).